ACS Catalysis

Research Article

pubs.acs.org/acscatalysis

Tailoring Gold Nanoparticle Characteristics and the Impact on Aqueous-Phase Oxidation of Glycerol

Scott M. Rogers,[†,‡] C. Richard A. Catlow,[†,‡] Carine E. Chan-Thaw,[§] Diego Gianolio,[∥] Emma K. Gibson,[†,‡] Anna L. Gould,[†,‡] Nan Jian,[⊥] Andrew J. Logsdail,[‡] Richard E. Palmer,[⊥] Laura Prati,[§] Nikolaos Dimitratos,[*,†,#] Alberto Villa,[*,§] and Peter P. Wells[*,†,‡]

[†]UK Catalysis Hub, Research Complex at Harwell, Rutherford Appleton Laboratory, Harwell Oxon, Didcot, OX11 0FA, United Kingdom

[‡]Department of Chemistry, University College London, 20 Gordon Street, London WC1H 0AJ, United Kingdom

[§]Dipartimento di Chimica, Università degli Studi di Milano, via Golgi 19, 20133 Milano, Italy

[∥]Diamond Light Source Ltd, Harwell Science and Innovation Campus, Chilton, Didcot OX11 0DE, United Kingdom

[⊥]Nanoscale Physics Research Laboratory, School of Physics and Astronomy, University of Birmingham, Edgbaston, Birmingham, B15 2TT, United Kingdom

[#]Cardiff Catalysis Institute, School of Chemistry, Cardiff University, Cardiff, CF10 3AT, United Kingdom

Supporting Information

ABSTRACT: Poly(vinyl alcohol) (PVA)-stabilized Au nanoparticles (NPs) were synthesized by colloidal methods in which temperature variations (−75 to 75 °C) and mixed H_2O/EtOH solvent ratios (0, 50, and 100 vol/vol) were used. The resulting Au NPs were immobilized on TiO_2 (P25), and their catalytic performance was investigated for the liquid phase oxidation of glycerol. For each unique solvent system, there was a systematic increase in the average Au particle diameter as the temperature of the colloidal preparation increased. Generation of the Au NPs in H_2O at 1 °C resulted in a high observed activity compared with current Au/TiO_2 catalysts (turnover frequency = 915 h^{-1}). Interestingly, Au catalysts with similar average particle sizes but prepared under different conditions had contrasting catalytic performance. For the most active catalyst, aberration-corrected high angle annular dark field scanning transmission electron microscopy analysis identified the presence of isolated Au clusters (from 1 to 5 atoms) for the first time using a modified colloidal method, which was supported by experimental and computational CO adsorption studies. It is proposed that the variations in the populations of these species, in combination with other solvent/PVA effects, is responsible for the contrasting catalytic properties.

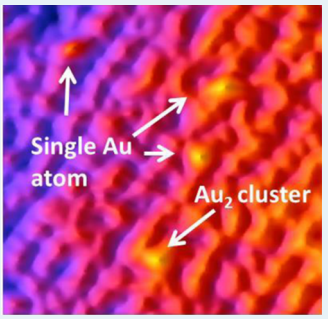

KEYWORDS: *gold nanoparticles, colloids, XAFS, glycerol oxidation, heterogeneous catalysis, aberration-corrected TEM*

INTRODUCTION

Tailored preparation of supported metal nanoparticles (NPs) is at the forefront of catalytic research. Characteristics of interest include metal particle size, shape and structure.[1−3] However, it is difficult to achieve fine control over these properties using typical synthesis approaches, that is, impregnation and precipitation.[4−6] The sol-immobilization method is a successful route for the synthesis of supported metal nanoparticles with tailored properties.[7,8] Colloidal methods have been studied for over 60 years and are able to prepare metal particles in a range of sizes (2−120 nm).[9−11] The particle size is dependent on the choice of stabilizer and the type of reducing agent used. The use of poly(vinyl alcohol) (PVA) as a stabilizing agent has become common in the preparation of metal nanoparticles <10 nm.[12−17] Colloids incorporating the use of PVA have been synthesized only as hydrosols, using water as the solvent, at room temperature. In terms of controlling the nanoparticle size during the reduction stage, attention has been focused on the gold concentration and the strength of the reductant used.[10,18,19] Understanding the effect of temperature and the surrounding solvent environment on the reduction process, and consequent particle characteristics, are crucially important.

It has been demonstrated that the catalytic properties of gold-NPs are highly dependent on the particle size, with minimal activity often observed at sizes >10 nm. At smaller particle sizes, Au is extremely active for CO oxidation,[20] hydrogenations,[21,22] and the selective oxidation of alkenes.[23−25] The origin of the reactive gold has been studied and attributed largely to the population of low-coordinated Au atoms as the active sites.[26] It is also well established that gold nanoparticles are effective for the selective oxidation of many alcohols.[16,27−29] Among the possible alcohols, glycerol is an attractive feedstock in the production of fine chemicals because it can be obtained as a byproduct from the production of biodiesel. As a highly

Received: April 10, 2015
Revised: May 21, 2015
Published: June 8, 2015

DOI: 10.1021/acscatal.5b00754
ACS Catal. 2015, 5, 4377−4384

functionalized molecule, there are many possible oxidation products; hence, a selective catalyst is required.[30] It is understood that the activity and selectivity toward glyceric acid is heavily affected by the metal nanoparticle size, with smaller metal nanoparticles <5 nm generating high turnover frequencies as a result of their high reaction rate.[16,28,29,31]

In the present study, we demonstrate how systematic approaches to designing nanoparticles can achieve both increased catalytic performance and durability in a manner that has not been previously reported. The work focuses on applying two modifications to an established sol-immobilization protocol, described elsewhere, for the preparation of titania supported gold nanoparticles:[13,16,32] (1) varying the temperature at which the colloid is generated and (2) applying different solvent systems through varied water/ethanol ratios. We characterize the Au particle size using transmission electron microscopy (TEM), aberration-corrected scanning transmission electron microscopy (STEM) and X-ray absorption fine structure (XAFS) and investigate the Au surface sites using CO-chemisorption with infrared (IR), corroborated by density functional theory (DFT) calculations. We performed catalytic tests in the liquid phase oxidation of glycerol to investigate the effects that temperature and the solvent used for nanoparticle preparation have on performance.

METHODS

Catalyst Preparation. A standard sol-immobilization method with temperature control was employed in the preparation of supported Au nanoparticles. $HAuCl_4 \cdot 3H_2O$ was used to prepare solutions with various H_2O/EtOH ratios of the desired gold concentration (1.26×10^{-4} M), to which solutions of PVA (1 wt % solution, Aldrich, M_w = 9000−10 000 g mol^{-1}, 80% hydrolyzed, PVA/Au (w/w) = 0.65) were added. Solutions of $NaBH_4$ (0.1 M) (>96%, Aldrich, $NaBH_4$/Au (mol/mol) = 5) were freshly prepared and added dropwise to each with stirring to form red-brown sols, depending on the solution temperature. After the complete reduction of gold species (30 min), the colloidal solutions were individually immobilized onto titania (P25, Degussa) under vigorous stirring conditions. The amount of support material required was calculated so as to give a final metal loading of 1 wt %. The mixture was acidified to pH 1−2 by sulfuric acid before it was stirred for 60 min. The slurry was filtered, and the resulting solid was washed thoroughly with distilled water, (2 L of doubly distilled water) to remove soluble impurities, and dried overnight at room temperature. The different H_2O/EtOH solvent ratios and temperatures at which each Au/TiO_2 catalyst was prepared, as well as an abbreviated name to be used throughout the paper, are presented in Table 1.

UV−Visible Spectroscopy. The colloidal hydrosols were analyzed by UV−vis spectroscopy to determine the position of the gold surface plasmon resonance band. UV−vis spectra (200−800 nm, Shimadzu UV-1800 spectrometer) of the Au sols were recorded in a quartz cuvette after 30 min of sol generation.

TEM and High Angle Annular Dark Field (HAADF) STEM Imaging. The surface morphology was investigated directly by imaging, with Au particle size and distribution the characteristics of interest. Samples for examination by TEM and aberration-corrected HAADF STEM were prepared by first dispersing the catalyst powder in high-purity ethanol using sonication. A 40 μL portion of the suspension was dropped onto a holey carbon film supported by a 300-mesh copper grid

Table 1. Applied Temperature and Solvent Ratios for Au/TiO_2 Catalyst Preparation

temp, °C	H_2O/EtOH solvent ratio (vol/vol)	sample abbreviation
1	100	A1
25	100	A2
50	100	A3
75	100	A4
−30	50	B1
0	50	B2
30	50	B3
−75	0	C1
−30	0	C2

before the solvent was evaporated. The samples for TEM and HAADF STEM were then examined using JEOL JEM 2100 EM and JEOL JEM 2100F STEM models, respectively. HAADF STEM analysis was performed in the Nanoscale Physics Research Laboratory at the University of Birmingham. The integrated HAADF STEM intensity was used to obtain the size of ultrasmall clusters, with large Au clusters functioning as a mass balance.[33−35]

XAFS. Au L_3-edge XAFS studies were carried out on the B18 beamline at the Diamond Light Source, Didcot, U.K. Measurements were performed in fluorescence mode using a QEXAFS setup with a fast-scanning Si(111) double crystal monochromator and a nine-element Ge detector. The time resolution of the spectra was 2 min/spectrum (k_{max} = 14). On average, 25 scans were acquired to improve the signal-to-noise level of the data. XAS data processing and extended X-ray absorption fine structure (EXAFS) analysis were performed using IFEFFIT with the Horae package (Athena and Artemis).[36,37] The amplitude reduction factor, s_0^2, was derived from EXAFS data analysis of an obtained Au foil spectrum to be 0.80, which was used as a fixed input parameter. The EXAFS data were fitted in R-space with a typical fit range of 1.15 < R < 5 Å.

Diffuse Reflectance Infrared Fourier Transform Spectroscopy (DRIFTS). FTIR spectra were obtained with an Agilent Cary 680 spectrometer at a spectral resolution of 2 cm^{-1} and accumulating up to 64 scans. For each experiment, the catalyst was placed in the sample holder and smoothed to leave a flat surface. The cell was purged with helium for 30 min before CO was introduced using a 10% CO/He mixture at a flow rate of 30 mL min^{-1} over a 5 min period. The gas was switched to helium for 30 min at a flow rate of 30 mL min^{-1} to remove gaseous and physisorbed CO from the catalyst surface.

Computer Simulations. DFT calculations were performed as implemented by the projector-augmented wave method (PAW).[38] Grid-based PAW uses a real-space grid, transforming the wave functions at the core to a smooth pseudowave function.[39] A converged grid spacing of 0.18 was used to represent numerically the wave function, and structural convergence was achieved when the forces on all atoms were found to be <0.01 eV $Å^{-1}$.

The geometries for small Au-CO clusters were taken from the previous work of Jiang and Xu,[40] and geometry optimizations were performed. The molecules investigated were Au_5CO, Au_4CO, Au_3CO, Au_2CO, $Au_2(CO)_2$, $Au(CO)_2$, and AuCO. Depending on the number of electrons in the system, spin-polarized (Au_5CO, Au_3CO, $Au(CO)_2$ and AuCO) and spin-paired (Au_4CO, Au_2CO, $Au_2(CO)_2$) calculations were performed for odd- and even-electron systems, respectively,

DOI: 10.1021/acscatal.5b00754
ACS Catal. 2015, 5, 4377−4384

with the generalized gradient approximation or Perdew, Burke and Ernzerhof as the exchange-correlation functional;[41] the residual minimization method, direct inversion in iterative subspace was used for convergence of the self-consistent cycle. For the odd-electron systems, a low-spin doublet configuration (μ = 1) was energetically preferable in all cases; a complete summary of the different spin states trialled and relative energies is provided in the Supporting Information (SI). The IR vibrational frequencies were calculated using finite-difference methods and compared with CO in the gas phase, and adsorbed at varying sites on Au (100) and (111) surfaces: namely, the atop, bridge, and hollow sites on the (100) surface; and the atop, bridge, hcp, and fcc sites on the (111) surface. The Au surface was modeled using a 5-layer-thick slab with 2D periodicity, using 1 k-point per 0.024 $Å^{-1}$ in the directions parallel to the surface plane (i.e., x and y). These studies, details of which are presented in the SI, show that the calculation of stretching frequencies may be limited to the contributions of the CO molecule and Au atoms that are directly bound to it, with all other atoms frozen, thus significantly reducing the computational load. Finally, we also considered the influence of charge on the vibrational frequencies to simulate for the effect of a charge-donating support such as TiO_2.

Glycerol Oxidation. A 0.3 M glycerol solution and the Au catalyst (substrate/total metal = 1000 mol/mol) were mixed in distilled water and NaOH (4:1 mol/mol NaOH/glycerol, total volume = 10 mL). The reactor was pressurized at 300 kPa of nitrogen, and the temperature was set to 50 °C. Once this temperature was reached, the gas supply was switched to oxygen, and the monitoring of the reaction started. The reaction was initiated by stirring. Samples were removed periodically and analyzed by high-performance liquid chromatography using a column (Alltech OA-10308, 300 mm_7.8 mm) with UV and refractive index detector aqueous H_3PO_4 solution (0.1 wt %) was used as the eluent. Products were identified by comparison with original samples. Recycling tests performed were under the same reaction conditions. The catalyst was recycled in the subsequent run after filtration without any further treatment. The recovery of the catalyst was >95% after each run. The volume of glycerol solution was adjusted in order to keep constant the substrate/metal ratio (1000 mol/mol).

RESULTS AND DISCUSSION

UV−Visible Characterization. The plasmon resonance band maximum, indicative of metal nanoparticles <10 nm, is presented in Table 2 for all Au catalysts. The band position ranged between 490 and 538 nm, influenced by both temperature and solvent during preparation. However, it is not possible to compare the effect of the different solvent systems on the position of the plasmon resonance band, as a result of differing dielectric properties of the solvent media.[42] Although each band is broad, it can be noted that there is a general shift to higher wavelength in the peak position of the plasmon band as the temperature to which the Au sols are generated increases. This indicates the formation of larger Au particles as the temperature of colloidal reduction increases, with the trend observed for all three solvent systems (H_2O shown in Figure 1, H_2O/EtOH and EtOH shown in Figure S1).

Table 2. Au Surface Plasmon Resonance Band Maximum and the Average Particle Diameter from TEM and EXAFS

Au/TiO_2 catalyst	UV maximum, nm	av TEM particle size, nm	av EXAFS particle size, nm
A1	500	2.0 ± 0.6	1.35
A2	490−500	2.3 ± 0.5	1.42
A3	500−510	2.8 ± 0.9	1.97
A4	538	3.3 ± 0.8	
B1	490−500	1.8 ± 0.5	1.18
B2	496	2.0 ± 0.6	1.24
B3	535−546	4.1 ± 1.8	
C1		2.4 ± 1.0	1.63
C2	516−520	2.9 ± 1.2	2.23

TEM. TEM was performed on all Au/TiO_2 catalysts to determine the particle size distribution. Representative TEM images and the derived histograms of the Au catalysts are presented in Figures 2 and S5. The average Au particle size and deviation for all Au catalysts are presented in Table 2. For the same solvent of preparation, the particle size analysis confirms that, as the temperature at which the Au colloid is formed decreases, a corresponding reduction in Au particle diameter and a narrowing of the overall distribution range is observed. This behavior is observed for all solvent systems investigated, with the water (A1 = 2.0 nm) and water−ethanol (B1 = 1.8 nm) environments yielding the smallest nanoparticles. To observe how the solvent environment during preparation affects particle size, it is possible to compare catalysts A1 against B2 as well as A2 against B3. These samples have comparable temperatures of colloidal reduction. There is little difference in average Au particle size when comparing A1 and B2, but there is an increase of 1.8 nm between the catalysts A2 and B3, which gives an indication that switching to a higher EtOH/H_2O solvent ratio increases the Au particle size during colloidal preparation. Switching to a pure EtOH solvent yields larger Au particles, regardless of the temperature, which could be attributed to the insoluble nature of PVA in EtOH, with full solubility achieved only if a few drops of H_2O are added during its preparation.

HAADF STEM. A1 and B1 catalysts were examined with HAADF STEM microscopy to investigate the presence of Au clusters that are too small to image with TEM. It was observed that ultrasmall Au clusters consisting of only a few atoms are present for the A1 catalyst (Figure 3), which were not, however, identified for B1. The quantitative analysis of the clusters' integrated HAADF STEM intensity shows that the ultrasmall clusters are of 1−5 Au atoms. For both Au catalysts, many Au clusters below 1 nm were recorded (Refer to Figures S2, S3).

XAFS Characterization. EXAFS was used to calculate the average Au particle size, as a representation of the whole sample. The first-shell EXAFS fitting parameters are shown in the SI, and the k^2-weighted magnitude Fourier transform data and corresponding fit presented in Figure 4 and Table S2. The EXAFS data shows that for all catalysts prepared, the Au environment is dominated by a primary Au coordination shell. The Au−Au first shell coordination numbers range between 7.7 and 11.2, all of which are lower than that found for bulk Au (12). The effect of temperature on the coordination number can be observed in Figure 5. Transforming the coordination number into a particle size can be performed using the approach of Beale et al.,[43] whose work simulated the average first shell coordination number versus the number of atoms for the first shell for each of the packing types. The average particle

DOI: 10.1021/acscatal.5b00754
ACS Catal. 2015, 5, 4377−4384

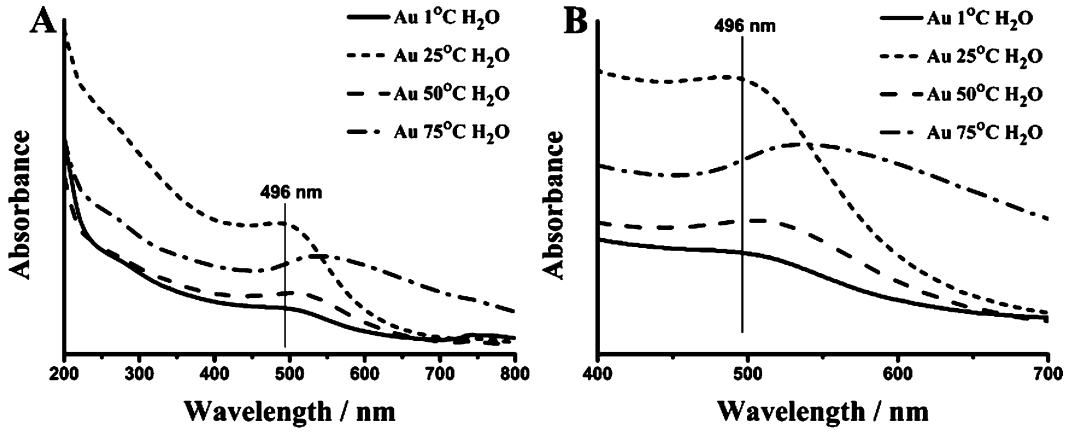

Figure 1. UV−vis spectra of Au sols prepared at different temperatures in H_2O: (A) full spectrum and (B) enlarged region for surface plasmon resonance band.

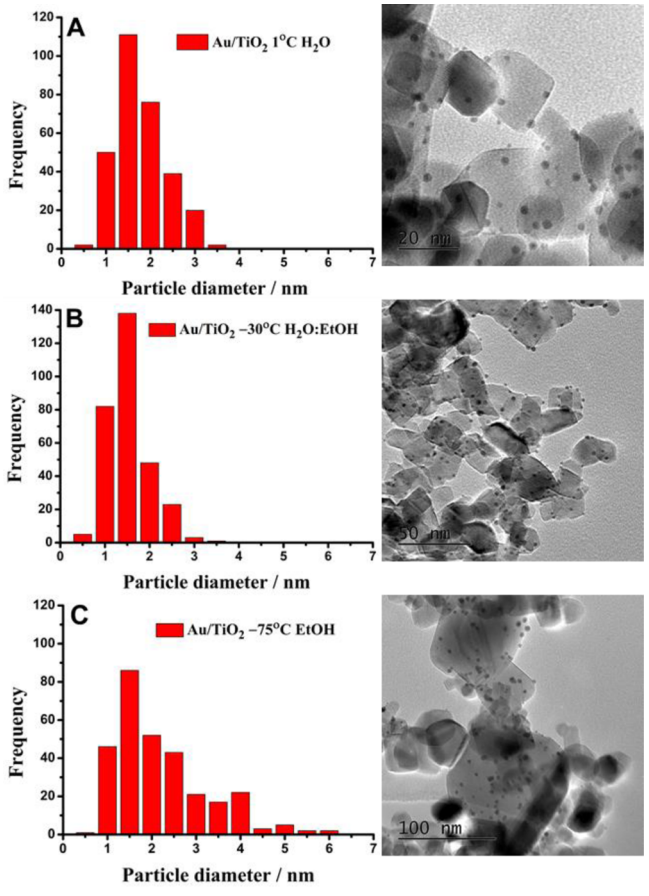

Figure 2. Representative TEM images and corresponding histograms of 1 wt % Au/TiO_2 catalysts: (A) A1, (B) B1, and (C) C1.

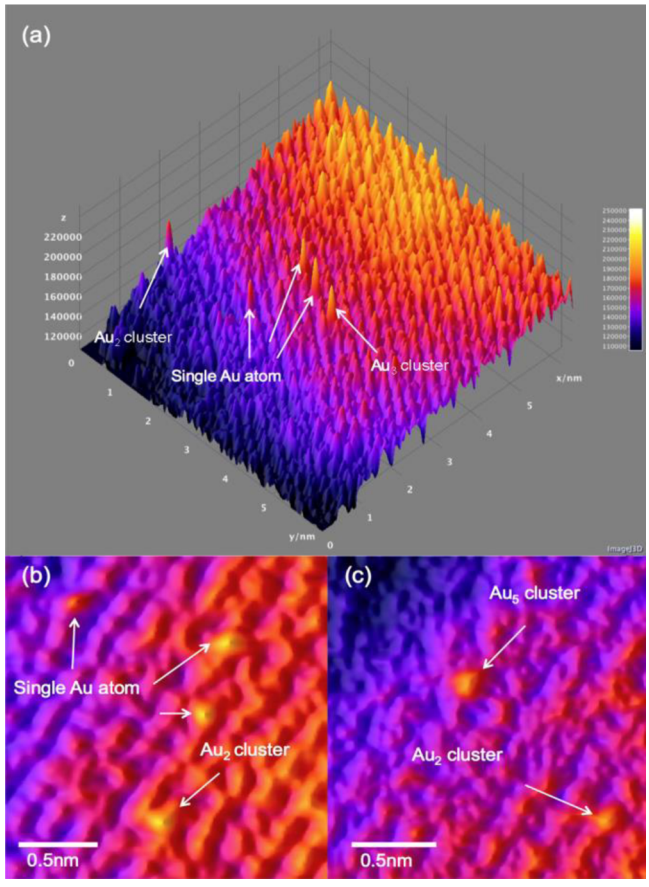

Figure 3. (a) 3D surface plot of A1 Au catalyst shows the ultrasmall clusters consisting of one and two Au atoms. (b) High resolution HAADF STEM images of single Au atom and Au2 cluster. (c) High resolution HAADF STEM images of Au2 and Au5 clusters.

size from TEM in our work, along with the particle size obtained from the first shell EXAFS coordination, are presented in Table 2. The values are based on the assumptions that the nanoparticles are spherical, face centered cubic, and <3 nm. As the diameter of the Au particles increases, the primary Au−Au radial distance (R) extends (2.81−2.84 Å), as is widely reported.[44] The trend for the Au particle diameter derived from the EXAFS supports the TEM analysis. The particle diameter obtained from EXAFS is smaller than that obtained from TEM due to EXAFS accounting for all the atoms that cannot be observed in microscopy.

DRIFTS. CO-adsorption spectra reveal a difference in surface sites and electronic properties between the Au samples. Figure 6A details the CO adsorption bands for catalysts A1 and A2, which have more defined CO adsorption bands compared with A3 (Figure 6B). With regard to the electronic properties at the Au/TiO_2 interface, previous literature has been used to assign the observed bands. The small band at ~2115 cm^{-1} present in the CO adsorption spectra of A1 and A2 can be assigned to $CO-Au^0$ species.[45] The broad band ~2040 cm^{-1} observed for

DOI: 10.1021/acscatal.5b00754
ACS Catal. 2015, 5, 4377−4384

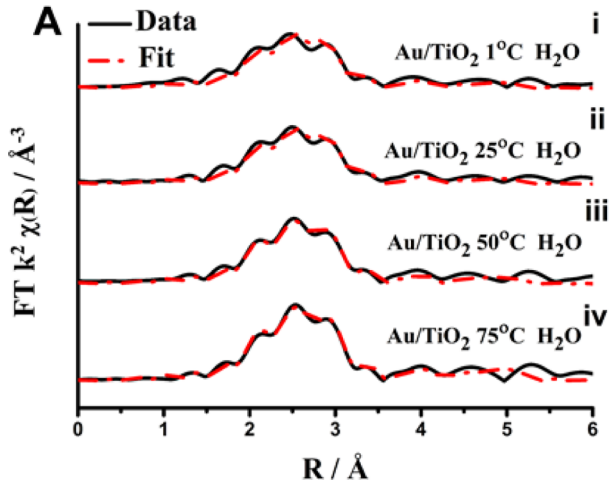

Figure 4. Magnitude component of the k^2-weighted Fourier transform data and corresponding fit for all the Au/TiO_2 catalysts prepared in a H_2O solvent (i. A1, ii. A2, iii. A3, iv. A4).

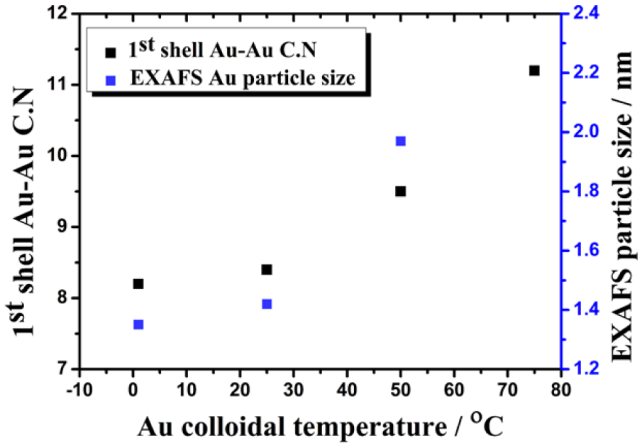

Figure 5. Effect of solvent temperature during Au colloidal formation in H_2O on the first shell EXAFS Au−Au coordination number and obtained Au particle size.

each sample is assigned to $CO-Au^{\delta-}$ as a result of electronic transfer from the reducible titania support to very small gold particles or clusters.[46,47] For A1 and A2 samples, it is evident from the asymmetric nature of this band that it comprises two different adsorption sites. The bands present below 1900 cm^{-1} are difficult to assign from the literature, with only clusters of $Au_5(CO)$ being reported with bands at this wavenumber.[40] The broadness associated with the CO adsorption bands for samples A3, B1, and C1 (Figure 6B) can be a result of the dipole coupling effect between neighboring CO molecules: when CO coverage is large, the dipoles between CO molecules couple, broadening the adsorption band. The sharp absorption bands observed in A1 and A2 provide evidence that there is limited coupling, confirming that the sites are more isolated.

Sample B1, in which the smallest average Au particle exists, did not produce the same CO-adsorption bands as described from the low temperature preparations in H_2O. Instead, the spectrum was consistent with that of the A3 catalyst, featuring two broad bands at ∼2040 and ∼1850 cm^{-1}, which is also observed for the samples prepared in pure EtOH (Figure 6B). The difference can be ascribed only to the influence of PVA on the gold species during the catalyst preparation in different

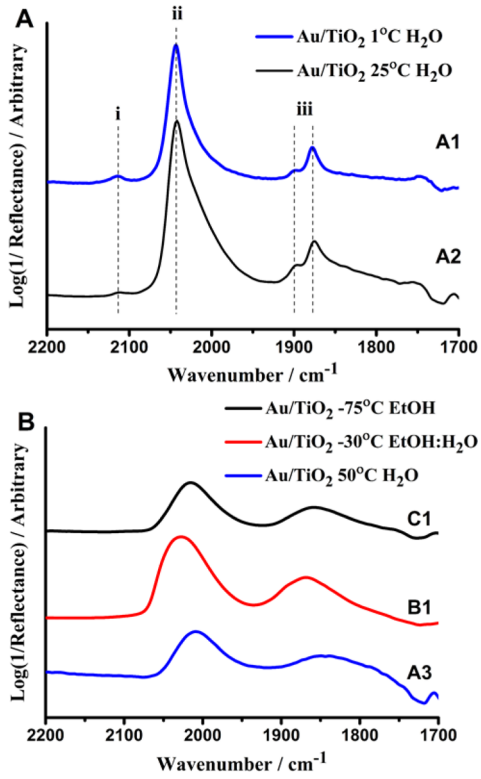

Figure 6. FTIR spectra from CO-adsorption studies onto different Au/TiO_2 catalysts: (A) A1, B1 and (B) C1, B1, and A3.

solvents. The interaction between PVA and the EtOH solvent appears detrimental to the available Au sites for CO adsorption. The samples of interest were not pretreated in any way to clean the catalyst surface or to modify the electronic properties; hence, in all cases, the stabilizing agent, PVA, may crucially inhibit the ability of each sample to adsorb CO at the surface. As a result, facile removal of the stabilizing agent has been widely investigated, with the aim of removing the protecting agent without affecting the structure of the catalyst.[33]

DFT Calculations. Geometry optimization and vibrational frequency analysis was performed on small Au_xCO clusters and for CO adsorbed at varying sites on (100) and (111). Our calculations show that the relevant vibrational modes in the IR spectra may be restricted to those relating to the CO molecule and directly bonded Au atoms, as shown in the ESI. The CO stretching frequencies for selected Au_xCO clusters and surface adsorption sites are given in Table 3.

From the results outlined, we see that the CO stretching frequencies when adsorbed on small gold clusters are lower than for gas-phase CO and similar to the slab calculations for which the CO molecule is adsorbed in an atop position, with a vibrational frequency of ∼2090 cm^{-1}. However, when CO binds in a bridging fashion, the vibrational frequency is shifted to considerably lower wavenumbers on the (100) and (111) surfaces. Both Au_3CO and Au_5CO molecules have CO positioned in a bridging arrangement, yet the CO stretching frequency for the Au_5CO is now much lower, at 1869.9 cm^{-1}. This result suggests that CO stretching frequencies below 1900 cm^{-1} may be assigned to bridging positions for the CO adsorbate on small Au clusters and may therefore correspond to the unusually distinct peaks highlighted in Figure 6.

To understand the influence of charge-donating supports, such as TiO_2, on the CO stretching frequencies, we also

DOI: 10.1021/acscatal.5b00754
ACS Catal. 2015, 5, 4377−4384

Table 3. Calculated CO Vibrational Frequencies of Gas-Phase CO, Small Au_xCO Clusters, and CO Adsorbed onto (100) and (111) Surface Slabs[a]

structure	adsorption site	CO vibrational frequency (cm^{-1})
CO	gas-phase	2134.6
AuCO	atop	1998.7
Au_2CO	atop	2108.3
$Au_2(CO)_2$	atop	2113.5
Au_3CO	bridge	2084.3
Au_4CO	atop	2096.1
Au_5CO	bridge	1869.9
$[Au_5CO]^-$	bridge	1767.2
Au (100)	atop	2085.4
Au (100)	bridge	1976.7
Au (100)	hollow	not stable
Au (111)	atop	2082.6
Au (111)	bridge	1998.7
Au (111)	hcp	1941.1
Au (111)	fcc	1944.9

[a]The (100) hollow site is unstable for CO adsorption.

negatively charged the Au_5CO molecule, reoptimized the geometry, and recalculated the vibrational frequencies. This procedure resulted in a significant red shift of the CO stretching frequency by 102.7 cm^{-1}, from 1869.9 to 1767.2.9 cm^{-1}. Given also the electronegative nature of Au, such a shift perhaps indicates that lower CO stretching frequencies in the experimental IR spectra could also arise from nanoparticle interactions with the substrate.

Glycerol Oxidation. Au/TiO_2 catalysts were evaluated for the liquid phase oxidation of glycerol under standard conditions: glycerol 0.3 M, 50 °C, 300 kPa O_2, glycerol/Au 1000 mol/mol, NaOH/glycerol 4 mol/mol. In Table 4, the

Table 4. Comparison of Au/TiO_2 Catalyst Activities in Glycerol Oxidation[a]

		selectivity (%)[c]				
Au/TiO_2 cat.	TOF (h^{-1})[b]	Glyc	Gly	Tartr	Lac	Form
A1	915	73	4	12	8	3
A2	663	74	4	12	6	1
A3	341	76	4	8	7	3
A4	161	79	6	2	7	4
B1	202	76	4	11	6	3
B2	95	78	5	9	5	3
B3	80	80	5	3	7	5
C1	130	78	4	9	6	3
C2	314	78	5	7	6	4

[a]Reaction conditions: alcohol/metal 1000/1 (mol/mol), 50 °C, pO_2 = 300 kPa, 1250 rpm. [b]TOF calculated after 15 min of reaction. [c]Selectivity at 90% conversion. Glyc = glycerate; Gly = glycolate; Tartr = tartronate; Lac = lactate; Form = formate.

activity and selectivity of Au catalysts prepared using different solvents and different temperatures are reported. All Au catalysts showed good selectivity to glyceric acid (73–80%). The Au/TiO_2 catalysts prepared in water showed the best catalytic performance compared with the alternative solvent systems, with A1 the most active catalyst (turnover frequency (TOF) of 915 h^{-1}). This value, compared with previously reported Au/TiO_2 catalysts, is high. Au/TiO_2 produced by deposition precipitation or synthesized using colloidal methods with tetrakis(hydroxymethyl)phosphonium chloride (THPC) as the stabilizing agent generated TOFs of 721 and 367 h^{-1}, respectively.[48] A2, A3, and A4 have significantly lower activities than A1 (TOF of 663, 341, and 161 h^{-1}, respectively), with time online analysis shown in Figure 7.

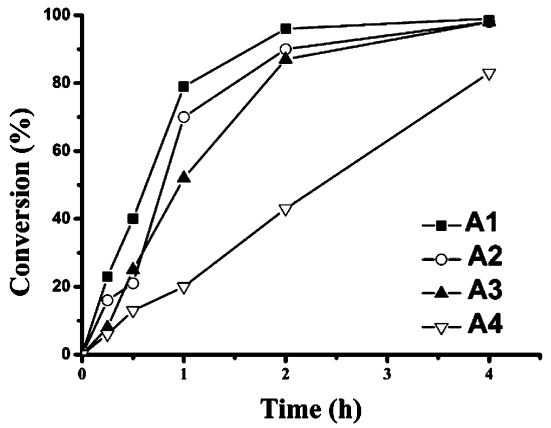

Figure 7. Reaction profile for Au catalysts prepared in H_2O.

Correlating the activity data for all Au catalysts with the average Au particle sizes showed that this is not the only parameter influencing the catalytic performance. Indeed, A1, A2, B1, B2, and C1 catalysts showed different catalytic behavior, despite the similar Au average particle diameter (1.8–2.4 nm). The difference can be attributed to two factors: (1) the population of very small Au clusters, as seen in A1 and (2) the interaction between protecting agent and solvent system, which is influenced by the temperature and the solvent in which the Au NPs are generated. It has previously been demonstrated that PVA affects the catalytic performance, as it is proposed that PVA can direct the adsorption of glycerol to Au active sites by interacting with the OH groups of glycerol.[49,50] There is an interesting result for the C series, in which the larger Au particle size catalyst, C2, has a greater activity than the smaller C1. We also attribute this trend to differences in the way PVA interacts with the Au colloids as a consequence of the low solubility of PVA in ethanol, which is exacerbated by the low temperature synthesis. We suggest that the presence of EtOH at the NP surface can also influence the adsorption of glycerol.

To explore the effect of the solvent used for the preparation of Au catalysts on their stability, we investigated the recyclability of the catalysts. The most active catalysts for each solvent (A1, B1, and C2) were chosen. The catalysts showed good stability after 10 runs, reaching full conversion after 4 h (Tables 5, 6, and S5). A1 showed a decreasing TOF between the first and second runs (915 and 652 h^{-1}). Afterward, the TOF remained constant in the successive eight runs (Table 5). The selectivity to glycerate decreased from 73% in the first run to 56% in the second run, during which a higher amount of tartronate was produced. This result can be attributed to the change in the average particle size of the A1 catalyst after the first run, with the aggregation of the very small Au clusters that were observed in HAADF STEM analysis. There was, indeed, an increase, from 2.0 to 3.7 nm, in the average Au particle diameter before and after the recycling tests by TEM. Au/TiO_2 prepared in $EtOH/H_2O$ and EtOH showed an increased TOF after the second run (Tables 6 and S5), which remained stable in the successive runs. The catalyst

DOI: 10.1021/acscatal.5b00754
ACS Catal. 2015, 5, 4377–4384

Table 5. Recycling Results Using the A1 Au Catalyst[a]

			selectivity (%)[c]			
A1[a]	TOF (h^{-1})[b]	conv. (%) after 4 h	Glyc	Gly	Tartr	Lac
run 1	915	98	73	4	12	8
run 2	652	98	56	6	22	9
run 3	678	99	57	6	25	9
run 4	659	98	59	6	23	9
run 5	649	98	57	9	24	6
run 6	657	97	56	11	23	7
run 7	638	98	57	10	24	7
run 8	652	98	58	11	24	6
run 9	649	98	56	10	22	6
run 10	632	99	58	12	22	7

[a]Reaction conditions: alcohol/metal 1000/1 (mol/mol), 50 °C, pO_2 = 300 kPa, 1250 rpm. [b]TOF calculated after 15 min of reaction. [c]Selectivity at 90% conversion. Glyc = glycerate; Gly = glycolate; Tartr = tartronate; Lac = lactate; Form = formate. [a]Prepared in H_2O at 1 °C.

Table 6. Recycling Results Using the B1 Au Catalyst[a]

			selectivity (%)[c]			
B1[a]	TOF (h^{-1})[b]	conv. (%) after 4 h	Glyc	Gly	Tartr	Lac
run 1	202	94	76	4	11	6
run 2	256	98	67	11	12	7
run 3	261	98	62	7	21	8
run 4	265	95	60	8	21	9
run 5	263	98	61	7	19	9
run 6	258	99	60	7	22	8
run 7	246	94	60	8	21	8
run 8	269	96	58	10	22	7
run 9	259	97	56	10	22	9
run 10	250	93	58	10	22	7

[a]Reaction conditions: alcohol/metal 1000/1 (mol/mol), 50 °C, pO_2 = 300 kPa, 1250 rpm. [b]TOF calculated after 15 min of reaction. [c]Selectivity at 90% conversion. Glyc = glycerate; Gly = glycolate; Tartr = tartronate; Lac = lactate; Form = formate. [a]Prepared in H_2O/EtOH at −30 °C.

stability is enhanced by the presence of the protecting agent, which is consistent with the lower activity observed for catalysts prepared in solvents containing EtOH, in which the EtOH and PVA influence the adsorption of glycerol. The catalytic performance of A1 and A3 catalysts was investigated at lower reaction temperature (25 °C) to minimize the aggregation of small clusters. As is shown in Tables S6 and S7, the stability of the catalysts was good, and selectivities of 81−87% to glycerate were obtained. These results demonstrate the applicability of supported gold catalysts in which the presence of gold clusters can enhance catalytic activity and can also be successfully reused without significant loss of activity.

CONCLUSIONS

This study demonstrates how Au NP characteristics can be tuned using solvent and temperature variations during colloidal synthesis and the impact this has on catalytic performance. The choice of temperature and solvent system proved crucial in dictating the performance for the liquid phase oxidation of glycerol, with the colloid generated at 1 °C in a water-only solvent giving the highest activity. This catalyst had a TOF of 915 h^{-1}, which compares favorably with other Au/TiO_2 catalysts in the literature that have been assessed under similar reaction conditions. The characterization of this catalyst, A1, demonstrated the presence of isolated ultrasmall Au clusters (1−5 atoms), as shown by HAADF STEM and supported by CO adsorption studies. The study also shows that catalysts with similar average Au particle diameters, A1 and B2, as identified by EXAFS and TEM - gave rise to different catalytic properties, with TOF values of 915 and 95 h^{-1}, respectively. This insight is of great importance when trying to elucidate accurate structure function relationships. This study links performance of Au/TiO_2 catalysts for glycerol oxidation to the population of specific cluster sizes and also indicates that reduced average particle diameter alone is not sufficient to promote the reaction. The interaction between the PVA and the Au NPs should not be ignored and may also influence the types/number of Au aggregates formed alongside affecting which sites are available.

ASSOCIATED CONTENT

Supporting Information

The Supporting Information is available free of charge on the ACS Publications website at DOI: 10.1021/acscatal.5b00754.

UV−vis spectra, TEM-HAADF images with supporting Au particle size distribution histograms, EXAFS fitting parameters, CO-chemisorption DRIFTS spectra, microwave plasma-atomic emission spectroscopy and computational information and additional catalytic data for glycerol oxidation (PDF)

AUTHOR INFORMATION

Corresponding Authors

*E-mail: DimitratosN@cardiff.ac.uk,.
*E-mail: alberto.villa@unimi.it.
*E-mail: peter.wells@rc-harwell.ac.uk.

Notes

The authors declare no competing financial interest.

ACKNOWLEDGMENTS

The authors wish to acknowledge the Diamond Light Source for provision of beamtime (SP8071). The RCaH are also acknowledged for use of facilities and support of their staff. Kristina Penman is thanked for performing the MP-AES measurements. Dr. A. J. Logsdail is grateful to the UCL Department of Chemistry and the Ramsay Memorial Trust for provision of a Ramsay Fellowship. UK Catalysis Hub is kindly thanked for resources and support provided via our membership of the UK Catalysis Hub Consortium and funded by EPSRC (Portfolio Grants EP I019693, EP/K014706/1, EP/K014668/1, EP/K014854/1, and EP/K014714/1). The authors acknowledge the use of the following high-performance computing facilities, and associated support services, in the completion of this work: ARCHER, via our membership of the UK HPC Materials Chemistry Consortium (EP/L000202); IRIDIS, provided by the Centre for Innovation; and UCL Legion.

REFERENCES

(1) Burda, C.; Chen, X.; Narayanan, R.; El-Sayed, M. A. *Chem. Rev.* **2005**, *105*, 1025−1102.
(2) Cushing, B. L.; Kolesnichenko, V. L.; O'Connor, C. J. *Chem. Rev.* **2004**, *104*, 3893−3946.
(3) Sun, Y.; Xia, Y. *Science* **2002**, *298*, 2176−2179.
(4) Schimpf, S.; Lucas, M.; Mohr, C.; Rodemerck, U.; Brückner, A.; Radnik, J.; Hofmeister, H.; Claus, P. *Catal. Today* **2002**, *72*, 63−78.

DOI: 10.1021/acscatal.5b00754
ACS Catal. 2015, 5, 4377−4384

(5) Enache, D. I.; Edwards, J. K.; Landon, P.; Solsona-Espriu, B.; Carley, A. F.; Herzing, A. A.; Watanabe, M.; Kiely, C. J.; Knight, D. W.; Hutchings, G. J. *Science* **2006**, *311*, 362−365.
(6) Carrettin, S.; McMorn, P.; Johnston, P.; Griffin, K.; Kiely, C. J.; Hutchings, G. J. *Phys. Chem. Chem. Phys.* **2003**, *5*, 1329−1336.
(7) Biella, S.; Prati, L.; Rossi, M. *J. Catal.* **2002**, *206*, 242−247.
(8) Prati, L.; Martra, G. *Gold Bull.* **1999**, *32*, 96−101.
(9) Roucoux, A.; Schulz, J.; Patin, H. *Chem. Rev.* **2002**, *102*, 3757−3778.
(10) Kimling, J.; Maier, M.; Okenve, B.; Kotaidis, V.; Ballot, H.; Plech, A. *J. Phys. Chem. B* **2006**, *110*, 15700−15707.
(11) Turkevich, J. *Gold Bull.* **1985**, *18*, 86−91.
(12) Shi, H.; Xu, N.; Zhao, D.; Xu, B.-Q. *Catal. Commun.* **2008**, *9*, 1949−1954.
(13) Porta, F.; Prati, L.; Rossi, M.; Coluccia, S.; Martra, G. *Catal. Today* **2000**, *61*, 165−172.
(14) Longenberger, L.; Mills, G. *J. Phys. Chem.* **1995**, *99*, 475−478.
(15) Ketchie, W. C.; Fang, Y. L.; Wong, M. S.; Murayama, M.; Davis, R. J. *J. Catal.* **2007**, *250*, 94−101.
(16) Porta, F.; Prati, L. *J. Catal.* **2004**, *224*, 397−403.
(17) Ketchie, W.; Murayama, M.; Davis, R. *Top. Catal.* **2007**, *44*, 307−317.
(18) Bond, G. C.; Thompson, D. T. *Catal. Rev.: Sci. Eng.* **1999**, *41*, 319−388.
(19) Bonnemann, H.; Richards, R. M. *Eur. J. Inorg. Chem.* **2001**, *2001*, 2455−2480.
(20) Haruta, M.; Kobayashi, T.; Sano, H.; Yamada, N. *Chem. Lett.* **1987**, *16*, 405−408.
(21) Sakurai, H.; Haruta, M. *Catal. Today* **1996**, *29*, 361−365.
(22) Sakurai, H.; Tsubota, S.; Haruta, M. *Appl. Catal., A* **1993**, *102*, 125−136.
(23) Inami, S. H.; Wood, B. J.; Wise, H. *J. Catal.* **1969**, *13*, 397−403.
(24) Sinha, A. K.; Seelan, S.; Tsubota, S.; Haruta, M. *Angew. Chem., Int. Ed.* **2004**, *43*, 1546−1548.
(25) Hughes, M. D.; Xu, Y. J.; Jenkins, P.; McMorn, P.; Landon, P.; Enache, D. I.; Carley, A. F.; Attard, G. A.; Hutchings, G. J.; King, F.; Stitt, E. H.; Johnston, P.; Griffin, K.; Kiely, C. J. *Nature* **2005**, *437*, 1132−1135.
(26) Janssens, T. W.; Clausen, B.; Hvolbæk, B.; Falsig, H.; Christensen, C.; Bligaard, T.; Nørskov, J. *Top. Catal.* **2007**, *44*, 15−26.
(27) Carrettin, S.; McMorn, P.; Johnston, P.; Griffin, K.; Hutchings, G. J. *Chem. Commun.* **2002**, 696−697.
(28) Carrettin, S.; McMorn, P.; Johnston, P.; Griffin, K.; Kiely, C.; Attard, G.; Hutchings, G. *Top. Catal.* **2004**, *27*, 131−136.
(29) Demirel-Gülen, S.; Lucas, M.; Claus, P. *Catal. Today* **2005**, *102−103*, 166−172.
(30) Sheldon, R. A.; Arends, I. W. C. E.; Dijksman, A. *Catal. Today* **2000**, *57*, 157−166.
(31) Dimitratos, N.; Lopez-Sanchez, J.; Lennon, D.; Porta, F.; Prati, L.; Villa, A. *Catal. Lett.* **2006**, *108*, 147−153.
(32) Pritchard, J.; Piccinini, M.; Tiruvalam, R.; He, Q.; Dimitratos, N.; Lopez-Sanchez, J. A.; Morgan, D. J.; Carley, A. F.; Edwards, J. K.; Kiely, C. J.; Hutchings, G. J. *Catal. Sci. Technol.* **2013**, *3*, 308−317.
(33) Wang, Z. W.; Palmer, R. E. *Nano Lett.* **2012**, *12*, 91−95.
(34) Wang, Z. W.; Toikkanen, O.; Yin, F.; Li, Z. Y.; Quinn, B. M.; Palmer, R. E. *J. Am. Chem. Soc.* **2010**, *132*, 2854−2855.
(35) Young, N. P.; Li, Z. Y.; Chen, Y.; Palomba, S.; Di Vece, M.; Palmer, R. E. *Phys. Rev. Lett.* **2008**, *101*, 246103.
(36) Ravel, B.; Newville, M. *J. Synchrotron Radiat.* **2005**, *12*, 537−541.
(37) Newville, M. *J. Synchrotron Radiat.* **2001**, *8*, 322−324.
(38) Blöchl, P. E. *Phys. Rev. B: Condens. Matter Mater. Phys.* **1994**, *50*, 17953−17979.
(39) Mortensen, J. J.; Hansen, L. B.; Jacobsen, K. W. *Phys. Rev. B: Condens. Matter Mater. Phys.* **2005**, *71*, 035109.
(40) Jiang, L.; Xu, Q. *J. Phys. Chem. A* **2005**, *109*, 1026−1032.
(41) Perdew, J. P.; Burke, K.; Ernzerhof, M. *Phys. Rev. Lett.* **1996**, *77*, 3865−3868.
(42) Underwood, S.; Mulvaney, P. *Langmuir* **1994**, *10*, 3427−3430.
(43) Beale, A. M.; Weckhuysen, B. M. *Phys. Chem. Chem. Phys.* **2010**, *12*, 5562−5574.
(44) Szczerba, W.; Riesemeier, H.; Thunemann, A. F. *Anal. Bioanal. Chem.* **2010**, *398*, 1967−1972.
(45) Dekkers, M. A. P.; Lippits, M. J.; Nieuwenhuys, B. E. *Catal. Lett.* **1998**, *56*, 195−197.
(46) Boccuzzi, F.; Chiorino, A.; Manzoli, M.; Andreeva, D.; Tabakova, T. *J. Catal.* **1999**, *188*, 176−185.
(47) Panayotov, D. A.; Burrows, S. P.; Yates, J. T.; Morris, J. R. *J. Phys. Chem. C* **2011**, *115*, 22400−22408.
(48) Dimitratos, N.; Villa, A.; Bianchi, C. L.; Prati, L.; Makkee, M. *Appl. Catal., A* **2006**, *311*, 185−192.
(49) Prati, L.; Villa, A. *Acc. Chem. Res.* **2014**, *47*, 855−863.
(50) Villa, A.; Wang, D.; Veith, G. M.; Vindigni, F.; Prati, L. *Catal. Sci. Technol.* **2013**, *3*, 3036−3041.

DOI: 10.1021/acscatal.5b00754
ACS Catal. 2015, 5, 4377−4384